Fault-tolerant Control of a Wind Turbine with a Squirrel-cage Induction Generator and Rotor Bar Defects

17th Int. Conference on Electrical Drives and Power Electronics The High Tatras, Slovakia 28-30 September, 2011

Vinko Lešić[1)], Mario Vašak[1)], Nedjeljko Perić[1)], Thomas M. Wolbank[2)] and Gojko Joksimović[3)]
[1)]Faculty of Electrical Engineering and Computing, University of Zagreb, Zagreb, Croatia
[2)]Faculty of Electrical Engineering and Information Technology, Vienna University of Technology, Vienna, Austria
[3)]Faculty of Electrical Engineering, University of Montenegro, Podgorica, Montenegro
vinko.lesic@fer.hr, mario.vasak@fer.hr, nedjeljko.peric@fer.hr, thomas.wolbank@tuwien.ac.at, joxo@ac.me

***Abstract*—Wind turbines are usually installed on remote locations and in order to increase their economic competence malfunctions should be reduced and prevented. Faults of wind turbine generator electromechanical parts are common and very expensive. This paper proposes a fault-tolerant control strategy for variable-speed variable-pitch wind turbines in case of identified and characterized squirrel-cage generator rotor bar defect. An upgrade of the torque control loop with flux-angle-based torque modulation is proposed. In order to avoid or to postpone generator cage defects, usage of pitch controller in the low wind speed region is introduced. Presented fault-tolerant control strategy is developed taking into account its modular implementation and installation in available control systems of existing wind turbines to extend their life cycle and energy production. Simulation results for the case of a 700 kW wind turbine and the identified rotor bar fault are presented.**

***Index Terms*—Wind Turbine Control, Torque Control, Generator-fault-tolerant control**

I. Introduction

Aspiration for finding adequate substitute for conventional fossil fuel power systems has a great impact on today political and economic trends and guidelines. Combining different branches of science and engineering, wind energy is recognized as the fastest-growing renewable energy source with an average growth rate of 27% in last 5 years [1]. It is green, inexhaustible, everywhere available but unreliable with poor power quality and as a result - expensive. The challenge is to make a control system capable of maximizing the energy production and the produced energy quality while minimizing costs of installation and maintenance.

Wind turbines are usually installed at low-turbulent-wind remote locations and it is important to avoid very costly unscheduled repairs. In order to improve reliability of wind turbines, different fault-tolerant control algorithms have been introduced [2], focused mainly on sensor, inverter and actuator faults. Focus here is on generator electromechanical faults, which are besides gearbox and power converters faults the most common in wind turbine systems [3]. Many installed wind turbines have squirrel-cage induction generator (SCIG) and about 20% to 30% of machine faults are caused by defects in rotor cage [4].

Rotor bar defect is caused by thermal fatigue due to cyclic thermal stress on the endring-bar connection which occurs because of different thermal coefficients of bars and lamination steel. As presented in [5], a monitoring system that is able to detect a developing bar defect is designed based on current signature analysis and offers the possibility to change from preventive to predictive maintenance and thus to significantly save costs.

Focus of this paper is to research and develop a fault-tolerant extension of the wind turbine control system that prevents the identified rotor bar defect from spreading. We introduce a fast control loop for flux-angle-based modulation of the generator torque, and a slow control loop that ensures the generator placement at a point that enables the fast loop to perform correctly and keeps the electrical energy production optimal under emergency circumstances.

This paper is organized as follows. The basic control strategy for a variable-speed variable-pitch wind turbine is presented in Section II along with normal wind turbine operating maps. In Section III a mathematical model of an SCIG is described explaining the theoretical basis used to form a control system extension. A fault-tolerant approach and control algorithm is proposed and described in Section IV that enables wind turbine operation in emergency state. Section V provides MATLAB/Simulink simulation results obtained with the proposed fault-tolerant control strategy.

II. Wind turbine control system

Variable-speed variable-pitch wind turbine operating area is parted into two regions (see Fig. 1): low wind speed region (region I), where all the available wind power is fully captured and high wind speed region (region II) where the power output is maintained constant while reducing the aerodynamic torque and keeping generator speed at the rated value.

The ability of a wind turbine to capture wind energy is expressed through a power coefficient C_P which is defined as the ratio of extracted power P_t to wind power P_V:

$$C_P = \frac{P_t}{P_V}. \tag{1}$$

The maximum value of C_P, known as Betz limit, is $C_{Pmax} = \frac{16}{27} = 0.593$. It defines the maximum theoretical capability

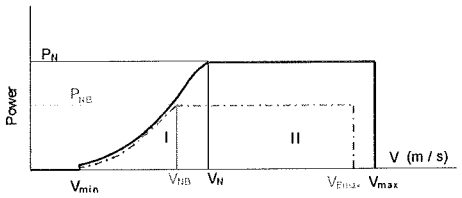

Fig. 1. Ideal power curve with maximum P_N and power curve due to developed fault with maximum P_{NB}.

of wind power capture. The real power coefficient of modern commercial wind turbines reaches values of about 0.48 [6]. Power coefficient data is usually given as a function of the tip-speed-ratio λ and pitch angle β (Fig. 2). Turbine power and torque are given by [7]:

$$P_t = C_P(\lambda,\beta)P_V = \frac{1}{2}\rho R^2 \pi C_P(\lambda,\beta)V^3, \quad (2)$$

$$T_t = \frac{P_t}{\omega} = \frac{1}{2}\rho R^3 \pi C_Q(\lambda,\beta)V^2, \quad (3)$$

where $C_Q = C_P/\lambda$, ρ, R, V and ω are torque coefficient, air density, radius of the aerodynamic disk of a wind turbine, wind speed and the angular speed of blades, respectively, and $\lambda = \frac{\omega R}{V}$.

Since the goal is to maximize the output power in low wind speed region, wind turbine must operate in the area where the power coefficient C_P is at its maximum value (or near it). This is achieved by maintaining λ and β on the values that ensure $C_P = C_{Pmax}$ [6]-[10], see Fig. 2. Therefore the generator torque and consequently the aerodynamic torque is determined by:

$$T_{gref} = \frac{1}{2\lambda_{opt}^3 n_s^3}\rho\pi R^5 C_{Pmax}\omega_g^2 = K_\lambda \omega_g^2, \quad (4)$$

where n_s is the gearbox ratio. This way the wind turbine operating points in low wind speed region are located at the maximum output power curve, called C_{Pmax} locus. This $T_{gref} = K_\lambda \omega_g^2$ torque controller (Fig. 3) can be easily realized using a simple look-up table.

Above designated rated wind speed, the task of the control system is to maintain the output power of the wind turbine constant. It can be done by reducing the aerodynamic torque and angular speed of blades by rotating them along their longitudinal axis (pitching). Consequently, the wind turbine power coefficient is reduced. A proportional-integral (PI) or proportional-integral-derivative (PID) controller with gain-

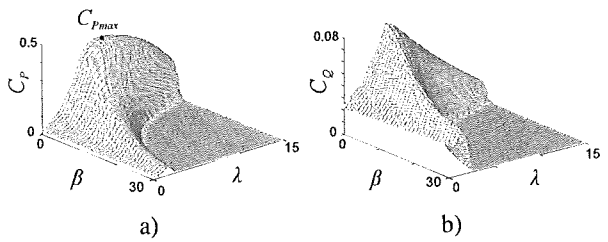

Fig. 2. Power a) and torque b) coefficients for an exemplary 700 kW variable-pitch turbine.

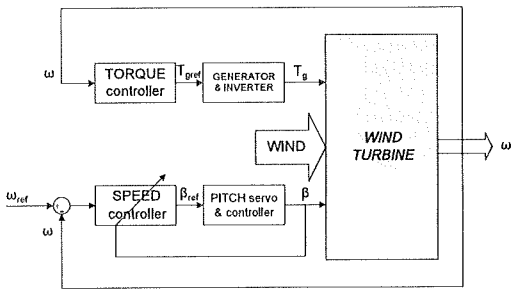

Fig. 3. Control system of a variable-speed variable-pitch wind turbine.

scheduling technique is often satisfactory for pitch control (Fig. 3).

III. Mathematical Model of an AC Machine

Mathematical model of an AC squirrel-cage induction machine can be represented in a two-phase (d,q) rotating coordinate system with following equations [11], [12]:

$$\bar{u}_s = R_s\bar{i}_s + \frac{d\bar{\psi}_s}{dt} + j\omega_e\bar{\psi}_s, \quad (5)$$

$$0 = R_r\bar{i}_r + \frac{d\bar{\psi}_r}{dt} + j(\omega_e - \omega_r)\bar{\psi}_r. \quad (6)$$

where bar notation represents a complex (d,q) vector, subscript s stator variables, subscript r rotor variables, i currents and R resistances. In a common rotating coordinate system stator variables are rotating with speed $\omega_e = 2\pi f$ and rotor variables with speed $\omega_e - \omega_r$, where f is the frequency of the AC voltage supplied to the stator, ω_g is the speed of rotor, $\omega_r = p\omega_g$, and p is the number of machine pole pairs. Flux linkages $\bar{\psi}_s$ and $\bar{\psi}_r$ are given by:

$$\bar{\psi}_s = L_s\bar{i}_s + L_m\bar{i}_r, \quad (7)$$

$$\bar{\psi}_r = L_m\bar{i}_s + L_r\bar{i}_r. \quad (8)$$

where $L_s = L_{s\sigma} + L_m$ is stator inductance, $L_r = L_{r\sigma} + L_m$ is rotor inductance, and L_m is mutual inductance. Parameters $L_{s\sigma}$ and $L_{r\sigma}$ are stator and rotor flux leakage inductances, respectively. Electromagnetic torque T_g is given by:

$$\bar{T}_g = -\frac{3}{2}pL_m\bar{i}_s \times \bar{i}_r. \quad (9)$$

By introducing a rotor field-oriented control (FOC), rotor flux linkage is in the rotating (d,q) frame fixed as

$$\bar{\psi}_r = \psi_{rd} + j0. \quad (10)$$

Magnetizing current that creates the rotor flux is then defined with

$$\bar{i}_{mr} = \frac{\bar{\psi}_r}{L_m} = \frac{\psi_{rd}}{L_m}. \quad (11)$$

By combining (6), (7), (8), (11) and by introducing rotor time constant parameter $T_r = \frac{L_r}{R_r}$, the following is derived:

$$i_{sd} = i_{mr} + T_r\frac{di_{mr}}{dt}, \quad (12)$$

$$\omega_{sl} = \omega_e - \omega_r. \quad (13)$$

where difference between the electrical and mechanical speed is a slip speed defined with $\omega_{sl} = \frac{i_{sq}}{T_r i_{mr}}$.

Finally, by combining (7), (8), (9) and (11) electromagnetic torque relation takes the form:

$$T_g = \frac{3}{2} p \frac{L_m^2}{L_r} i_{mr} i_{sq} = k_m i_{mr} i_{sq}. \quad (14)$$

Relation (14) is the key equation for FOC of an induction machine and using rotor FOC i_{sd} and i_{sq} are fully decoupled. Magnetizing current vector i_{mr} is not suitable for fast control action influencing torque because of the time lag T_r and is therefore kept constant in the sub-nominal speed operating region. Torque is controlled only by q stator current component - i_{sq}.

Voltage-controlled machine (Fig. 4) is usually more suitable than the current-controlled so by substituting (7), (8), (11), (12) into (5) stator voltage vector components u_{sd} and u_{sq} are obtained:

$$u_{sd} = k_a i_{sd} + \sigma L_s \frac{di_{sd}}{dt} - \frac{1}{T_r} \frac{L_m^2}{L_r} i_{mr} - \omega_e \sigma L_s i_{sq}, \quad (15)$$

$$u_{sq} = R_s i_{sq} + \sigma L_s \frac{di_{sq}}{dt} + \omega_e \frac{L_m^2}{L_r} i_{mr} + \omega_e \sigma L_s i_{sd}. \quad (16)$$

where $k_a = (R_s + \frac{L_m^2}{L_r^2} R_r)$ and $\sigma = (1 - \frac{L_m^2}{L_s L_r})$. Relations (15) and (16) show that d and q coordinates are not fully decoupled and changing the voltage value in one axis, affects also the other. Elements with ω_e represent machine back-electromotive force (EMF). Since it would be very complicated to control these coupled voltages, a decoupling method is applied (see [12]). By introducing correction voltages Δu_{sd} and Δu_{sq}, fully decoupled relations are derived:

$$u_{sd} + \Delta u_{sd} = k_a i_{sd} + \sigma L_s \frac{di_{sd}}{dt}, \quad (17)$$

$$u_{sq} + \Delta u_{sq} = R_s i_{sq} + \sigma L_s \frac{di_{sq}}{dt}. \quad (18)$$

These equations are now suitable for further design of the control loop and PI controllers are chosen with integral time constants $T_{Id} = \sigma L_s / k_a$ for d-current, $T_{Iq} = \sigma L_s / R_s$ for q-current and gain K_r. As previously mentioned, in the normal machine operating region i_{sd} is kept constant and $i_{mr} = i_{sd}$ is implied. Finally, closed loop dynamics can now be represented as first-order lag system with transfer function:

$$\frac{T_g(s)}{T_{g\_REF}(s)} = \frac{i_{sq}(s)}{i_{sq\_REF}(s)} = \frac{1}{1 + \tau s}, \quad (19)$$

where τ is a time constant defined with $\tau = \frac{\sigma L_s}{K_r}$.

Minimum and maximum torque references that can be applied to closed loop system, implied by the back EMF and maximum inverter voltage U_{max}, are defined respectively with:

$$T_1 = \frac{1}{K_r k_g} (-U_{max} - k_e \omega_e) - T_0, \quad (20)$$

$$T_2 = \frac{1}{K_r k_g} (U_{max} - k_e \omega_e) + T_0, \quad (21)$$

where $k_g = k_m i_{sd}$, $k_e = L_s i_{sd}$ and T_0 is the torque starting point for the transient. Notice that back EMF supports torque reduction and aggravates torque restoration. Because of $i_{mr} = i_{sd}$ the slip speed is proportional to the torque (or i_{sq} current):

$$\omega_{sl} = \frac{i_{sq}}{T_r i_{mr}} = \frac{1}{T_r k_m i_{mr}^2} T_g = k T_g. \quad (22)$$

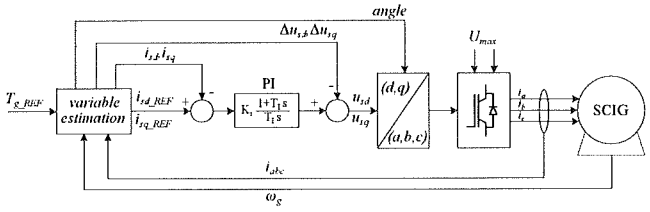

Fig. 4. Field-oriented control loop.

IV. FAULT-TOLERANT CONTROL

Previous sections have described most widely adopted wind turbine control strategies, as well as mathematical model of the generator. This section is dedicated for further improvement of control strategies in order to disable or to postpone generator fault development and to achieve maximum energy production under emergency conditions at the same time. A work that is focused on stator winding inter-turn short circuit faults for synchronous machines also appeared recently [13]. For now, detected generator fault triggers a turbine safety device and leads to a system shut-down. Whole unscheduled repair process requires significant amounts of money and the situation is even worse for off-shore wind turbines. Not to mention opportunity costs of turned-off wind turbine.

To avoid thermal stress of the defected rotor bar, currents flowing through it should be less than currents flowing through the healthy ones. The magnitude of currents in rotor bar is sinusoidal and it is determined by the machine magnetic flux. Speed at which the flux rotates along the rotor circumference is the generator slip speed defined with (13). Flux affects the damaged rotor bar only on a small part of its path as it moves along the circumference and is denoted with $\Delta\theta = \theta_2 - \theta_1$, which corresponds to the angular width of the damaged bar, see Fig. 5. Our primary goal is to reduce the electrical and thermal stress reflected through currents and corresponding generator torque in that angle span to the maximum allowed safety value T_{gf}. The value T_{gf} is determined based on fault identification through machine fault monitoring and characterization techniques, together with flux angles θ_1 and θ_2 [5].

Torque is therefore modulated based on the machine flux angular position with respect to the damaged part as shown in Fig. 5. When the flux in angle θ approaches the angle span $\Delta\theta$, the torque is reduced to the maximum allowed value T_{gf} defined with a fault condition. After the flux passes it, the torque is restored to the right selected value T_{g_nonf}. The value T_{g_nonf} is determined such that the average machine torque

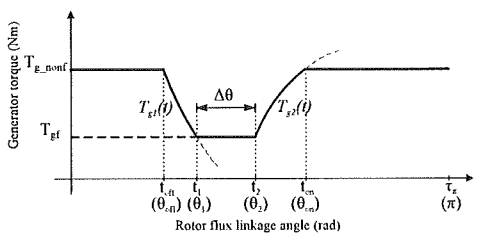

Fig. 5. Torque modulation due to a fault condition. In brackets are angles attained at denoted time instant.

is maintained on the optimum level, taking into account the machine constraints. Procedure is then periodically executed, with period equal π (or τ_π in time domain), since the flux influences the faulty part with its north and south pole in each turn.

Using the described FOC algorithm with decoupling procedure the generator is modelled as first-order lag system as mentioned in the previous section. Torque transients from Fig. 5 are therefore defined as exponential functions, decrease and increase respectively:

$$T_{g1}(t) = \mathrm{e}^{-\frac{t}{\tau}}\left(T_{g\_nonf} - T_1\right) + T_1 \quad (23)$$

$$T_{g2}(t) = T_2 - \mathrm{e}^{-\frac{t}{\tau}}\left(T_2 - T_{gf}\right) \quad (24)$$

Slip speed of the generator is defined as

$$\omega_{sl}\left(T_g\left(t\right)\right) = \frac{\mathrm{d}\theta}{\mathrm{d}t}, \quad (25)$$

from which the angle is obtained:

$$\theta(t) - \theta(0) = \int_0^t \omega_{sl}\left(T_g\left(t\right)\right)\mathrm{d}t = \int_0^t kT_g\left(t\right)\mathrm{d}t. \quad (26)$$

Desired T_{gf} is reached with transient (23) at certain time t_1 and desired T_{g_nonf} is reached with transient (24) at certain time t_{on}:

$$T_{gf} = \mathrm{e}^{-\frac{t_1}{\tau}}\left(T_{g\_nonf} - T_1\right) + T_1, \quad (27)$$

$$T_{g\_nonf} = T_2 - \mathrm{e}^{-\frac{t_{on}}{\tau}}\left(T_2 - T_{gf}\right) + T_2. \quad (28)$$

The angle span which has passed during the torque reduction determines the angle θ_{off} at which the transition has to start in order to reach the torque T_{gf} at angle θ_1 due to the finite bandwidth of the torque control loop. In the same way torque restoration transient determines the angle θ_{on} at which the torque T_{g_nonf} is fully restored. Finally, θ_{off} is derived from (20), (26) and (27):

$$\theta_{off} = \theta_1 - k\tau\left(T_{g\_nonf} - T_{gf} - T_1 \ln a\right), \quad (29)$$

where $\ln a = \ln\frac{T_{gf}-T_1}{T_{g\_nonf}-T_1}$. In the same way, θ_{on} is obtained as:

$$\theta_{on} = \theta_2 + k\tau\left(T_{gf} - T_{g\_nonf} - T_2 \ln b\right), \quad (30)$$

where $\ln b = \ln\frac{T_2-T_{g\_nonf}}{T_2-T_{gf}}$.

If the torque value T_{g_nonf} can be restored at some angle then the following relation holds:

$$\theta_{on} - \theta_{off} \leqslant \pi. \quad (31)$$

Putting (29) and (30) into (31), the following is obtained for condition (31):

$$-k\tau\left(T_1 \ln a + T_2 \ln b\right) \leqslant \pi - \Delta\theta. \quad (32)$$

Because of large inertia of the whole drivetrain, generator and blade system, described torque oscillations (reduction and restoration) are barely noticeable on the speed transient, such that the wind turbine shaft perceives the mean torque value:

$$T_{av} = \frac{1}{\tau_\pi}\int_0^{\tau_\pi} T_g \mathrm{d}t. \quad (33)$$

Mean value of the generator torque from Fig. 5 is then given by:

$$T_{av} = \frac{\pi - 2k\tau\left(T_1 \ln a + T_2 \ln b\right)}{k\tau_\pi}, \quad (34)$$

with

$$\tau_\pi = \frac{\pi - \Delta\theta + k\tau\left(T_1 \ln a + T_2 \ln b\right)}{kT_{g\_nonf}} - \\ -\tau\left(\ln a + \ln b\right) + \frac{\Delta\theta}{kT_{gf}}. \quad (35)$$

Equation (31) (or (32)) is not satisfied if the speed ω_g is large enough (or if there is a large rotor path under fault influence). In that case the torque modulation is given with Fig. 6 and peak torque T_g^* is attained at angle θ^*:

$$\theta_2 - \pi + k\tau\left(T_{gf} - T_g^* - T_2 \ln b^*\right) = \\ = \theta_1 - k\tau\left(T_g^* - T_{gf} - T_1 \ln a^*\right) \quad (36)$$

where $\ln a^* = \ln\frac{T_{gf}-T_1}{T_g^*-T_1}$ and $\ln b^* = \ln\frac{T_2-T_g^*}{T_2-T_{gf}}$. Values T_g^* and θ^* can be obtained from:

$$k\tau\left(T_1 \ln a^* + T_2 \ln b^*\right) = \Delta\theta - \pi \quad (37)$$

$$\theta^* = \theta_1 - k\tau\left(T_g^* - T_{gf} - T_1 \ln a^*\right). \quad (38)$$

Mean value of the generator torque from Fig. 6 (i.e. in case when (31) is not satisfied) is now given by

$$T_{av} = \frac{\pi - k\tau\left(T_1 \ln a^* + T_2 \ln b^*\right)}{k\tau_\pi^*}, \quad (39)$$

with

$$\tau_\pi^* = -\tau\left(\ln a^* + \ln b^*\right) + \frac{\Delta\theta}{kT_{gf}}. \quad (40)$$

Concludingly, if (32) is fulfilled, the resulting average torque is given with (34); if not, then the resulting average torque is given with (39). On the boundary, i.e. for equality in (31) or (32), both (34) and (39) give the same torque T_{av}, such that $T_{av}(\omega_g)$ is continuous. The maximum available torque T_{g_nonf} is the nominal generator torque T_{gn}. Replacing T_{g_nonf} in (34) with the nominal generator torque T_{gn} gives the maximum available average torque under fault characterized with $\Delta\theta$ and T_{gf}. Fig. 7 shows an exemplary graph of available speed-torque points under machine fault, where the upper limit is based on relations (32), (34) and (39) with $T_{g\_nonf} = T_{gn}$. Dashed area denotes all available average generator torque values that can be achieved for certain generator speed.

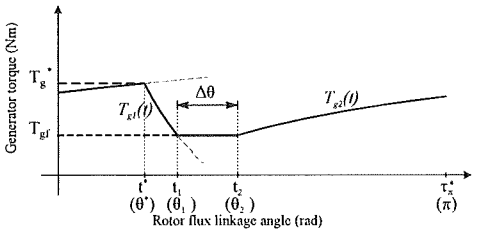

Fig. 6. Torque modulation due to a fault condition when T_{g_nonf} cannot be restored.

From Fig. 7 it follows that up to the speed ω_{g1} it is possible to control the wind turbine in the faulty case without sacrificing power production. However, from that speed onwards it is necessary to use blades pitching in order to limit the aerodynamic torque and to keep the power production below optimal in order to suppress the fault from spreading. The speed control loop is modified such that instead of reference ω_n the reference ω_1 (in case of gearbox, $\omega_1 = \omega_{g1}/n_s$) is selected. This activates pitch control once the right edge of the feasible-under-fault optimal torque characteristics is reached. The optimal power point on $T_{av}(\omega_g)$, which is always on the upper edge of the dashed area, may deviate from this point and thus further improvements in power production outside the point $(\omega_{g1}, T_{av}(\omega_{g1}))$ may be obtained by using maximum power tracking control along the curve of maximum T_{av} in the speed span $[\omega_{g1}, \omega_{gn}]$. The interventions in classical wind turbine control that ensure fault-tolerant control are given in Fig. 8. Algorithms of the slow and the fast fault-tolerant control loop are given in the sequel.

1) Fault-tolerant control algorithm, slow loop:

I. If $T'_{gref} \leq T_{gf}$, disable the fast loop and pass T'_{gref} to the torque controller;

II. Compute T_{g_nonf} from (20), (21), (34) and (35) such that $T_{av}(\omega_g) = T'_{gref}$; if $T_{g\_nonf} > T_{gn}$, set $T_{g\_nonf} = T_{gn}$;

III. If (32) is fulfilled set $\theta_{start} = \theta_{off} \bmod \pi$ and $\theta_{end} = \theta_{on}$ else compute θ^* from (38) and set $\theta_{start} = \theta^* \bmod \pi$, $\theta_{end} = \theta_2$ and $T_{g\_nonf} = T_2$;

IV. Compute ω_{g1} as a speed coordinate of the intersection point of $T_{av}(\omega_g)$ and of the normal wind turbine torque controller characteristics, compute $\omega_1 = \omega_{g1}/n_s$ and set $\omega_{ref} = \omega_1$.

2) Fault-tolerant control algorithm, fast loop:

I. On the positive edge of logical conditions:

- $\theta > \theta_{start}$ set $T_{gref} = T_1$,
- $\theta > \theta_1$ set $T_{gref} = T_{gf}$,
- $\theta > \theta_2$ set $T_{gref} = T_2$,
- $\theta > \theta_{end}$ set $T_{gref} = T_{g\_nonf}$.

V. Simulation Results

This section provides simulation results for a 700 kW MATLAB/Simulink variable-speed variable-pitch wind turbine

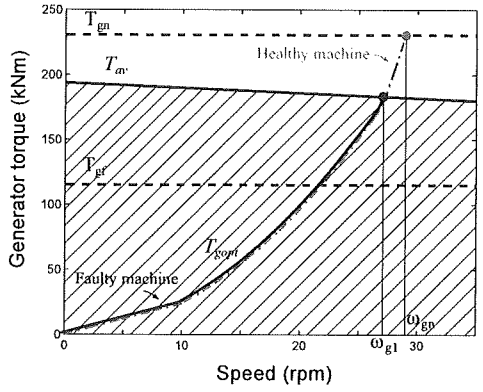

Fig. 7. Available torque-speed generator operating points under fault condition (shaded area). Full line is the achievable part of the wind turbine torque-speed curve under faulty condition. Dash-dot line is the healthy machine curve.

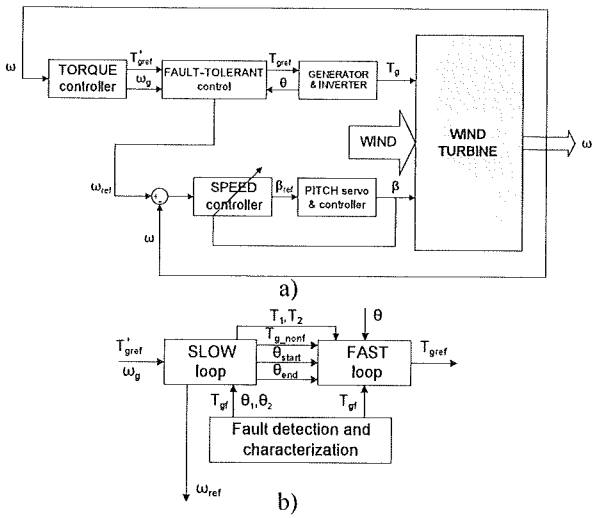

Fig. 8. a) Control system of wind turbine with fault-tolerant control strategy. b) Enlarged fault-tolerant control block.

model with a two-pole 5.5 kW SCIG scaled to match the torque of 700 kW machine. Generator parameters are: $L_s = L_r = 0.112$ H, $L_m = 0.11$ H, $R_s = 0.3304\ \Omega$, $R_r = 0.2334\ \Omega$ and PI controller gain is $K_r = 1$. Turbine parameters are: $C_{Pmax} = 0.4745$, $R = 25$ m, $\lambda_{opt} = 7.4$, $\omega_n = 29$ rpm, $T_{tn} = 230.5$ kNm with gearbox ratio $n_s = 105.77$. Maximum voltage of DC-link is $U_{max} = 214$ V. Fault is simulated between flux angles $\theta_1 = \frac{\pi}{2}$ and $\theta_2 = \frac{\pi}{2} + \frac{\pi}{5}$, with $T_{gf} = 0.5 T_{gn}$ and presented fault-tolerant control algorithm is applied. Results in Fig. 9 show how the wind turbine behaves in healthy and faulty condition for a linear change of wind speed through the entire wind turbine operating area.

Fig. 10 shows the fault-tolerant control system reaction to the fault that is identified at $t = 40$ s for the case when the average generator torque under fault $T_{av}(\omega_g)$ can be equal to the required torque T'_{gref} for the incurred speed ω_g, i.e. the optimum speed-torque point is for the occurred fault in the dashed area of Fig. 7, above the line $T_g = T_{gf}$.

Fig. 11 shows the fault-tolerant control system reaction to the fault identified at $t = 40$ s for the case when the incurred healthy machine speed-torque operating point falls out of the dashed area of Fig. 7. In this case blade pitching is used in the faulty condition to bring the speed-torque operating point into $(\omega_{g1}, T_{av}(\omega_{g1}))$.

Fig. 12 shows the influence of fast loop reference switching on generator currents (and torque). This way the time needed for torque transients is reduced to minimum possible value keeping wind turbine in low-energy production operation as little as possible under emergency circumstances.

VI. Conclusions

This paper introduces a fault-tolerant control scheme for variable-speed variable-pitch wind turbines with a squirrel-cage generator. We focus on generator rotor bar defect that can be characterized at early stage of development. A simple extension of the conventional control structure is proposed that prevents the fault propagation while power delivery under fault

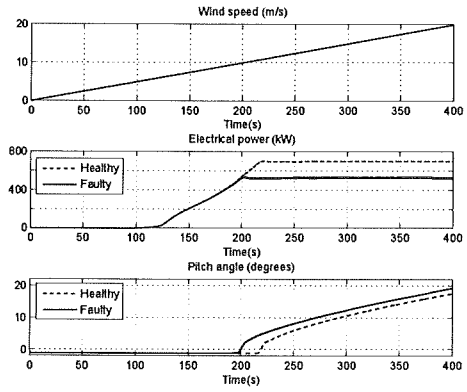

Fig. 9. Wind turbine power production and pitch angle for healthy and faulty conditions.

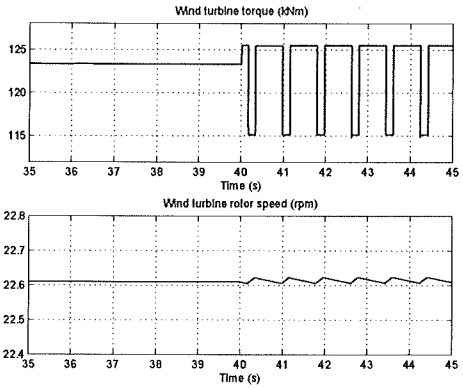

Fig. 10. Generator torque modulation and wind turbine speed when $T_{g\_nonf} < T_{gn}$. Fault occurs at 40 s.

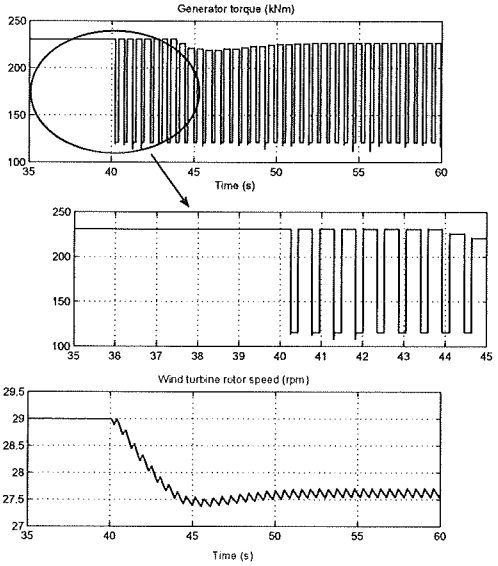

Fig. 11. Generator torque modulation and wind turbine speed when $T_{g\_nonf} = T_{gn}$. Fault occurs at 40 s.

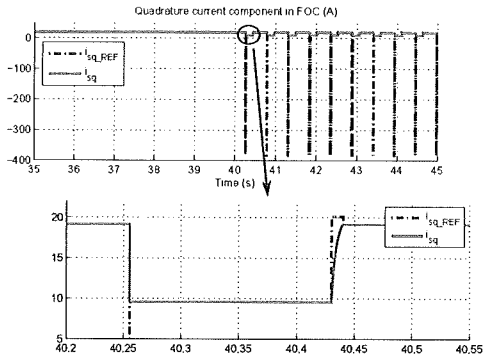

Fig. 12. Quadrature current component.

is deteriorated as less as possible compared to healthy machine conditions.

ACKNOWLEDGEMENT

This work has been supported by the European Commission and the Republic of Croatia under grant FP7-SEE-ERA.net PLUS ERA 80/01.

REFERENCES

[1] World Wind Energy Association. (2010). World wind energy installed capacity [Online]. Available: http://www.wwindea.org

[2] S. Pourmohammad, A. Fekih, "Fault-Tolerant Control of Wind Turbine Systems - A Review",*Proc. of the 2011. IEEE Green Technologies Conference (IEEE-Green)*, April 2011.

[3] Z. Daneshi-Far, G. A. Capolino, H. Henao, "Review of Failures and Condition Monitoring in Wind Turbine Generators", *XIX International Conference on Electrical Machines - ICEM 2010*, September 2010.

[4] A. H. Bonnet and C. Yung, Increased efficiency versus increased reliability, *IEEE Industry Applications Magazine*, vol.14, no.1, pp.29-36, 2008.

[5] G. Stojičić, P. Nussbaumer, G. Joksimović, M. Vašak, N. Perić and T. M. Wolbank, "Precise Separation of Inherent Induction Machine Asymmetries from Rotor Bar Fault Indicator", *8th IEEE International Symposium on Diagnostics for Electrical Machines, Power Electronics & Drives, SDEMPED*, 2011.

[6] M. Jelavić, N. Perić, I. Petrović, M. Kajari and S. Car, "Wind turbine control system", *Proc. of the 7th Symposium on Power System Management, HO CIGRE*, November 2006, pp. 196-201.

[7] F. D. Bianchi, H. De Battista and R. J. Mantz, *Wind Turbine Control Systems - Principles, Modelling and Gain Scheduling Design.*, London, England: Springer, ISBN 1-84628-492-9, 2007.

[8] T. Burton, D. Sharpe, N. Jenkins and E. Bossanyi *Wind Energy Handbook*, England: John Wiley & Sons, ISBN 0-471-48997-2, 2001.

[9] L. Y. Pao and K. E. Johnson, "Control of Wind Turbines: Approaches, Challenges, and Recent Developments", *IEEE Control Systems Magazine* vol. 31, no. 2, April 2011, pp. 44-62.

[10] F. Blaabjerg, F. Iov, R. Teodorescu and Z. Chen. "Power Electronics in Renewable Energy Systems" *Proc. of the 12th International Power Electronics and Motion Control Conf. (EPE-PEMC 2006)*, 2006.

[11] W. Leonhard, *Control of Electrical Drives*, Berlin, Germany: Springer Verlag, ISBN 3-540-41820-2, 2001.

[12] M. P. Kazmierkowski, F. Blaabjerg and R. Krishnan, *Control in Power Electronics - Selected Problems*, San Diego, California: Academic Press, An imprint of Elsevier Science, ISBN 0-12-402772-5, 2002.

[13] V. Lešić, M. Vašak, T. M. Wolbank, G. Joksimović, N. Perić, "Fault-Tolerant Control of a Blade-pitch Wind Turbine With Inverter-fed Generator", *20th IEEE International Symposium on Industrial Electronics, ISIE*, June 2011, pp. 2097-2102.